

# Tailored Frequency Conversion Makes Infrared Light Visible for Streak Cameras

Carolin Lüders<sup>1,\*</sup> Jano Gil-Lopez<sup>2,†</sup> Markus Allgaier,<sup>2,3,‡</sup> Benjamin Brecht<sup>2,§</sup> Marc Aßmann,<sup>1,¶</sup> Christine Silberhorn,<sup>2,||</sup> and Manfred Bayer<sup>1,\*\*</sup>

<sup>1</sup>Experimentelle Physik 2, Technische Universität Dortmund D-44221, Germany

<sup>2</sup>Integrated Quantum Optics, Institute for Photonic Quantum Systems (PhoQS), Universität Paderborn, Warburger Str. 100, Paderborn 33098, Germany

<sup>3</sup>Department of Physics and Oregon Center for Optical, Molecular, and Quantum Science, University of Oregon, Eugene, Oregon 97403, USA

(Received 10 June 2022; revised 21 October 2022; accepted 23 December 2022; published 31 January 2023)

Streak cameras are one of the most common and convenient devices to measure pulsed emission, e.g., from semiconductor lightsources with picosecond time resolution. However, they are most sensitive in the visible range and possess low or negligible efficiency in the infrared and telecom regime. In this work, we present a frequency conversion based on sum-frequency generation that converts infrared to visible signals while preserving their temporal properties, making them detectable with a streak camera. We demonstrate and verify the functionality of our device by converting the emission from a quantum dot laser.

DOI: 10.1103/PhysRevApplied.19.014072

## I. INTRODUCTION

Many applications require measuring the temporal properties of optical emission from semiconductors: verifying single-photon emission [1] or quantifying quantum coherence [2] for quantum information tasks; analyzing carrier and phonon dynamics [3]; observing the lasing dynamics of alternative laser candidates [4] or studying cooperative effects in quantum dots, such as super-radiance [5] and superfluorescence [6].

For these tasks, detection methods with a temporal resolution in the range of pico- to femtoseconds are needed. These can be distinguished into techniques that measure the pulse form via intensity autocorrelation [e.g., optical autocorrelation [7], spectral shearing interferometry (SPIDER) [8], frequency-resolved optical gating (FROG) [9]]; these methods typically require large field intensities], techniques working at the single-photon level but not delivering short pulse forms (e.g., the Hanbury-Brown Twiss setup for  $g^{(2)}$  measurements [10]) and techniques resolving (ultra)short pulse forms with single-photon sensitivity (optical Kerr gating [11], frequency up-conversion sampling [12], electro-optic shearing interferometry [13], and streak cameras [14]). Also there are various types of single-photon detectors with time resolutions on the order

of 100 ps [15]. Another kind of information is obtained by pump-probe schemes measuring time-resolved reflectivity or absorption of the material [3].

While a plethora of techniques allow access to the temporal envelope of pulses at the single-photon level, only streak cameras [16,17] allow simultaneous access to other degrees of freedom, e.g., spatial [18] or spectral in combination with a spectrometer. Particularly in the semiconductor community, streak cameras are popular, as they allow measuring photon correlations with ca. 2-ps time resolution, resolving the small coherence times of semiconductor light sources [19–23].

However, measuring technologically relevant wavelengths beyond 1000 nm (e.g., the telecommunication wavelengths around 1310 and 1550 nm, or midinfrared wavelengths beyond 2 microns) poses additional challenges for these methods. The wavelength range of Kerr gating is limited to around 1100 nm by material properties and the wavelength of the gating pulse [24,25]; streak cameras are constrained by the photocathode material and do not possess sufficient quantum efficiency in the telecom range [26] (e.g., conventional S1 photocathodes have a radiant sensitivity of ca.  $2 \times 10^{-4}$  mA/W at 1500 nm, corresponding to a quantum efficiency of  $1.6 \times 10^{-7}$  [27], whereas InP/(In, Ga)As photocathodes have a radiant sensitivity of ca. 1 mA/W at 1500 nm, corresponding to a quantum efficiency of  $8 \times 10^{-4}$  [28]); and electro-optic shearing interferometry relies on single-photon detection. Of all types of single-photon detectors, superconducting nanowire single-photon detectors are most promising, combining sensitivity for telecom wavelengths together with a good time resolution. Although the best individual timing jitter demonstrated for these detectors under lab

\* carolin.lueders@tu-dortmund.de

† jangil@campus.uni-paderborn.de

‡ markusa@uoregon.edu

§ benjamin.brecht@uni-paderborn.de

¶ marc.assmann@tu-dortmund.de

|| christine.silberhorn@uni-paderborn.de

\*\* manfred.bayer@tu-dortmund.de

conditions amounts to about 3 ps [29], timing jitters on the order of at least 20 ps are more common [15,30] and are the state of the art in commercial systems. This available timing jitter is at least one order of magnitude worse than the one of a streak camera. Also, nanowire detectors possess a dead time in the nanosecond range while streak cameras have no dead time at all.

Apart from these, for the infrared, techniques based on frequency up-conversion sampling are the only viable candidates to date. In frequency up-conversion sampling, the investigated light is mixed with a bright pulsed pump laser in a nonlinear optical material and converted to the sum frequency of the involved fields. The intensity of the up-converted light can be measured with any detector while varying the time delay between the signal field and pump pulses, thereby reconstructing the temporal shape of the signal with a time resolution given by the pump-pulse duration. In semiconductor physics, this method has been applied, e.g., to carrier dynamics in carbon nanotubes [31], superfluorescent emission of excitons in ZnTe [32], and to  $g^{(2)}$  measurements of a confined polariton structure [33].

While frequency up-conversion can be applied to a wide range of wavelengths, given a suitable nonlinear material, pump laser, and detector, it relies on scanning the delay between the pump pulse and the weak signal field. This necessarily yields long acquisition times, since at any one position of the pump pulse, only a small part of the signal field is sampled.

Another approach where the temporal shape of the input field is preserved by the up-conversion with a cw pump has been demonstrated in Refs. [34,35]. However, in that approach, single-photon-counting avalanche photodiodes (SPADs) were used together with a time-correlated single-photon-counting (TCSPC) board for time-resolved measurements, which gave a time resolution of 40–50 ps. In general, SPADs provide a timing jitter of around 40 to several 100 ps [36], being at least one order of magnitude worse than a streak camera.

In this work, we present a method that combines up-conversion and streak cameras, joining the advantages of both techniques and the high time resolution of the streak camera, in order to measure quantum dot emission in the infrared. To this aim, we design and demonstrate a sum-frequency generation (SFG) process in lithium niobate, which converts an infrared input signal to visible wavelengths while preserving its temporal properties. Notably, this conversion is realized with a cw laser, foregoing the need for ultrashort pump pulses as no scanning is involved. Further, only certain defined spatial polarization modes are converted, which reduces background compared to direct detection in the IR.

Our work is based on techniques presented in Ref. [26], where the information about the temporal shape of the signal was completely lost during the SFG. Here, we design

the SFG to precisely conserve the temporal shape of the signal light.

To prove the correct reproduction of the pulse shape, we first convert quantum dot emission at a wavelength of 900 nm where we can detect both the original and the converted light with the streak camera. We show that the conversion process acts as a filter, selecting only the desired spectral band of the quantum dot emission, thus further reducing spurious background photons. Using a 40-mm-long crystal, we achieve up to 14% internal conversion efficiency, which is, in principle, sufficient to improve overall detection efficiencies about twofold. We then demonstrate a proof-of-concept realization of a SFG process for higher wavelength regimes, which shows that the method can be flexibly adapted while retaining its noise-filtering properties.

## II. SUM-FREQUENCY GENERATION FOR UP-CONVERSION DETECTION

SFG is a three-wave-mixing second-order nonlinear process.

In this process, a signal and pump field with frequencies  $\omega_s$  and  $\omega_p$  produce a third output field with frequency  $\omega_o = \omega_s + \omega_p$ .

The spectral properties of the output are given by the transfer function and depend upon the properties of the nonlinear material used to produce SFG with the phase-matching function and the pump used for the process. The transfer function can be written as [37]

$$\Phi(\omega_s, \omega_p) = \int d\omega_s d\omega_p \alpha(\omega_p) \phi(\omega_s + \omega_p), \quad (1)$$

where  $\alpha(\omega_p)$  is the envelope of the pump field and  $\phi(\omega_s + \omega_p)$  the phase-matching function of the process. As depicted in Fig. 1, the transfer function determines the input-output spectral, and thus, by virtue of the Fourier relationship between time and frequency, also the temporal, characteristics of the SFG.

In general, a nonengineered transfer function does not ensure the conservation of the signal field spectral characteristics (spectral bandwidth and time duration) upon conversion. It is therefore useful to engineer a transfer function that faithfully reproduces the original signal characteristics at the converted wavelengths. This is realized by a careful adaption of the pump and phase-matching properties. For instance, for an angle of 45°, the transfer function, cf. Fig. 1, produces a 1:1 ratio between signal and output fields and is the ideal condition to achieve a faithful conversion. Note that the spectral acceptance band of the SFG is defined by the phase-matching bandwidth and angle in this configuration. Special care must be taken to ensure that the process accepts the complete quantum dot emission, while simultaneously rejecting as much unwanted background as possible. We demonstrate such a process in the

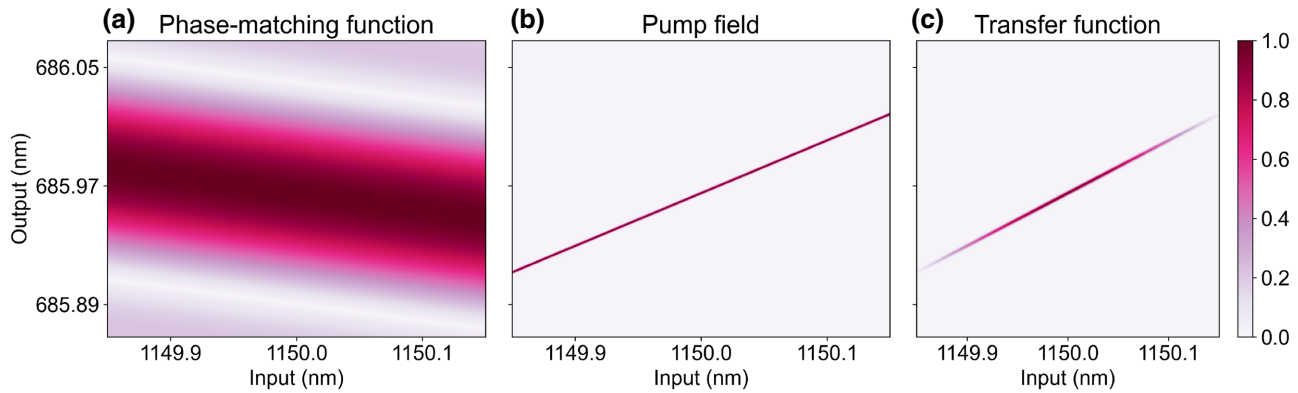


FIG. 1. (a) Amplitude of the phase-matching function for the engineered type-II SFG process. (b) Amplitude of the pump field for a continuous-wave laser. (c) Amplitude of the transfer function for a process using the phase-matching function in (a) and the pump in (b). For more information see the text.

following. In our experiment, the process does not alter the spectrum of the signal during translation to a different wavelength and, in turn, conserves the temporal properties. Indeed, assuming a perfect cw pump and sufficient acceptance bandwidth, our process translates the central frequency of any signal without altering the temporal characteristics and the time resolution is only limited by the streak camera at around 2 ps. Note that the length of our waveguide of 40 mm and the field confinement make it possible to foregoe high peak pump powers to achieve efficient up-conversion and enables us to use a cw pump laser.

With these considerations in mind, we design two SFG processes in periodically poled titanium in-diffused lithium niobate waveguides, matched to the available quantum dots. The first process transforms quantum dot light at around 900 nm, which is visible to the streak camera, and serves to verify that the temporal and spectral properties are conserved upon conversion. The second process is designed for quantum dot light that is invisible to the streak camera and demonstrates the flexibility of our approach; its phase-matching and transfer functions are depicted in Fig. 1. Both processes are engineered to work at around 190 °C to avoid the effects of photorefraction [38].

### III. CONVERSION OF NEAR-INFRARED WAVELENGTHS

#### A. Experimental setup

In order to validate the correct replication of the temporal properties, in a first step we convert quantum dot light at a wavelength still accessible for the streak camera. The experimental setup for this task is shown in Fig. 2. The continuous-wave pump beam (1712 nm, spectral width < 1 MHz) is provided by an OPO (Argos 2400). The signal (898 nm) is emitted by Al<sub>0.9</sub>GaIn<sub>36</sub>As quantum dots

inside of a GaAs  $\lambda$  microcavity, forming a planar micro-laser. 26 mirror pairs of GaAs/AlAs create the upper part of the resonator and 33 mirror pairs form the lower one. This microlaser is held in a cryostat at 9 K and excited nonresonantly at 740 nm in a confocal scheme with a 50 $\times$  microscope objective by a pulsed Ti:sapphire laser with a repetition rate of 75 MHz. The excitation laser is filtered from the signal with a 900-nm band pass with 10-nm FWHM (Thorlabs FB900-10). After being combined on a dichroic mirror, both the signal and the pump field are focused into the 40-mm-long LiNbO<sub>3</sub> waveguide with a poling period of 19  $\mu$ m for the type-0 SFG process. The waveguide is kept at a temperature of 190 °C. After the waveguide, a 600-nm band pass with 10-nm FWHM (Thorlabs FB600-10), which is slightly tilted to adapt to the converted wavelength, removed the pump and any remaining unconverted signal. We detect the SFG up-converted light (589 nm) on a streak camera (Hamamatsu C5680-25) equipped with a S-20 photocathode, having a quantum efficiency of 0.72% at 900 nm and 8.16% at 590 nm, corresponding to a cathode radiant sensitivity of 5.22 and 38.84 mA/W, respectively. The device's

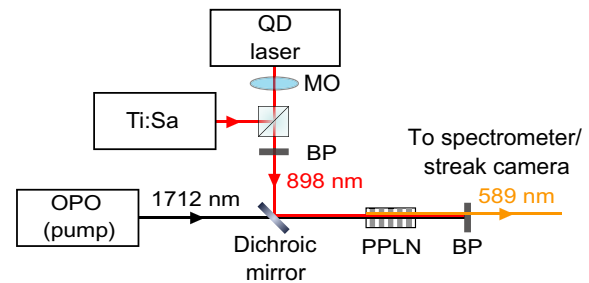


FIG. 2. Experimental setup for frequency conversion. Ti:Sa, Ti:sapphire laser; MO, microscope objective; OPO, optical parametric oscillator; PPLN, periodically poled LiNbO<sub>3</sub> waveguide; BP, bandpass filter.

deflection circuit is synchronized to the Ti:sapphire laser repetition rate. For measuring spectra below 1000 nm, we use an Acton SP-2500i spectrometer equipped with a PyLoN:400BR\_eXcelon CCD camera, having a resolution of 0.05 nm at 435.8 nm according to the manufacturer. For wavelengths above 1000 nm, a Stellarnet EPP2000-NIR-(In, Ga)As spectrometer is used. It provides a resolution of 5 nm according to the manufacturer.

## B. Results

The original and the converted spectra of the quantum dot laser are compared in Fig. 3.

The unconverted spectrum consists of several peaks, corresponding to different modes of the microcavity. The most intense peak lies at 898.3 nm with a FWHM of 0.06 nm. In contrast to that, the converted spectrum shows only a single peak at 589.1 nm with a FWHM of 0.06 nm. We observe almost no conversion of the less intense peaks. As desired, the SFG acts as a noise filter, selecting only the specific wavelength region for which the phase-matching condition is fulfilled. For this mode, the spectral width is apparently retained during conversion; however, the detected width of this extremely narrow signal is very close to the resolution of the spectrometer. Nevertheless, since the temporal shape is preserved as explained below and shown in Fig. 5, it is reasonable to assume that the spectral width is preserved as well.

As a figure of merit, we characterize the internal conversion efficiency of the process by measuring the depletion of the quantum dot signal. To this aim, the unconverted signal spectrum is recorded after the waveguide, both with the pump open and blocked. From the spectra, we obtain the peak intensities  $P_{\text{blocked}}$  and  $P_{\text{open}}$ . With these quantities, we calculate the internal conversion efficiency via

$$\text{Efficiency} = 1 - \frac{P_{\text{open}}}{P_{\text{blocked}}}. \quad (2)$$

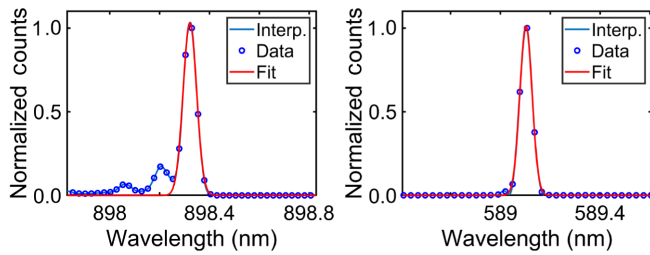


FIG. 3. Original (left) and converted (right) spectra of the quantum dot emission. Blue dots, data; red line, Gaussian fit; blue line, interpolant as guide for the eye. Only the main peak is converted, whereas spurious side peaks are suppressed, showing the selective properties of the SFG process. The intensities are normalized. They are not directly comparable due to different detection sensitivities, filters, and losses in the setup.

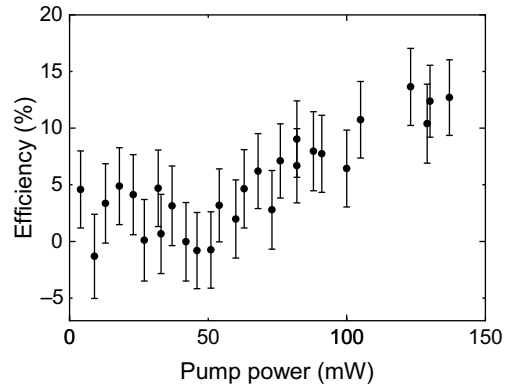


FIG. 4. Pump-power dependence of the internal conversion efficiency. The pump power is measured after the waveguide. The excitation power of the quantum dots has been kept constant.

Its dependence upon pump power is shown in Fig. 4, with the pump power being measured after the waveguide.

According to this, the internal efficiency of the upconversion depends linearly on pump power in the range of powers between 50 and 140 mW. Below 50 mW, the difference between the signal with pump blocked and unblocked is too weak to be discerned from fluctuations occurring during the measurement. For sufficiently high powers, a saturation behavior is expected to occur but is not observed within the investigated range of powers. Within this range, the internal efficiency reaches almost up to 14%. This seemingly small number is more than counteracted by the detection efficiencies of the streak camera, which are 0.72% at around 900 nm and 8.16% at 590 nm, respectively, yielding a potential twofold increase in detection efficiency when compared to direct detection at the original emission wavelength. Due to additional losses in the setup (e.g., absorption in optical elements, nonperfect waveguide coupling), this is not demonstrated at this point. Instead, care is taken to demonstrate the faithful conversion of the temporal and spectral properties of the signal upon conversion.

The key results of our proof-of-principle experiment are the temporal pulse shapes of the original and the up-converted quantum dot emission, measured with the streak camera. The spatially integrated streak-camera images are compared in Fig. 5. In the unconverted case, all the spectral components of the signal shown in Fig. 3 (left) are sent to the streak camera, bypassing the waveguide. The used pump power is 70 mW after the waveguide to ensure being well within the linear regime.

The pulse shape of the quantum dot emission varies with excitation power. We find that the up-converted pulse shape reproduces the original one accurately. Thus, the temporal properties of the quantum dot emission are preserved during the conversion, even while spurious side peaks in the spectral domain are not converted.

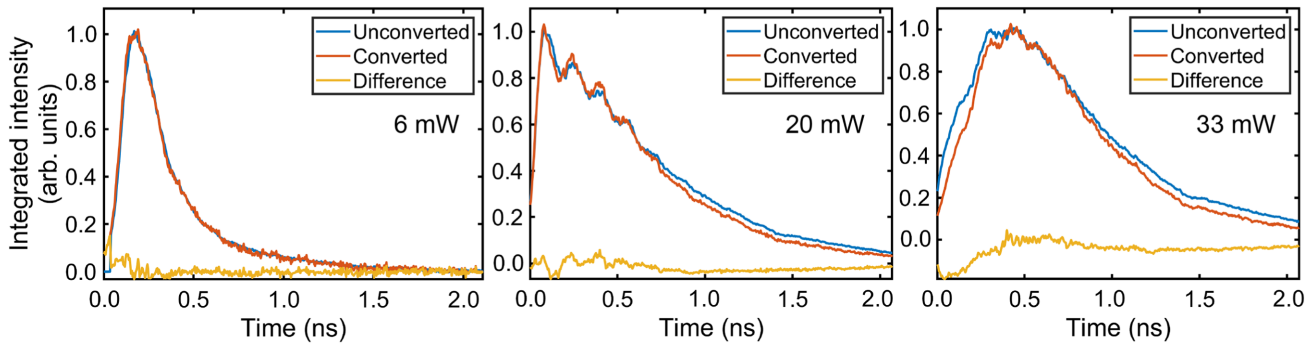


FIG. 5. Temporal wave forms of the original (blue) and converted (red) quantum dot emission for different excitation powers. The curves are normalized and shifted so that their maxima coincide. Yellow: intensity difference. The frequency conversion process accurately retains the temporal properties of the input light.

Only for higher excitation powers, the converted pulse is slightly shorter than the unconverted one, while still preserving the shape qualitatively. This might be caused by the spectral components of the signal that are not converted and are not removed by the 900-nm-band pass, as they lie too closely to the main peak. For higher excitation powers, these might also be detected by the streak camera and might arrive later than the emission from the main peak.

Notably, for excitation powers higher than 16 mW, an oscillation in the temporal wave form appears. This oscillation supposedly stems from relaxation dynamics induced by the interaction of the QD states with the population reservoir of wetting-layer states. This turn-on dynamics of quantum dot lasers has also been observed and modeled in Ref. [39] on a similar time scale. Let us emphasize here that our technique is able to resolve this fast dynamics having a period of 150 ps.

To analyze the signal-to-noise properties, Fig. 6 shows a cut through the streak-camera image along the spatial position of maximum intensity for 6-mW excitation power and without background subtraction. The signal-to-noise ratio or dynamic range is still 2.2 times better for the unconverted signal than for the converted one in this case. This is reasonable since we use a pump power of 70 mW where the internal conversion efficiency is ca. 5%, but it can be improved by using a higher pump power. The inset depicts the tail of both pulses for long times without normalization of the intensity. The background intensity is equal for the converted and the unconverted signal. Apparently, no significant additional noise is produced in the conversion. It is known that the up-conversion of anti-Stokes Raman photons that are scattered from the cw pump into the wavelength range of the signal can cause a constant background [35,40], but this is not visible here. According to Ref. [40], this Raman background becomes less relevant for a pump with longer wavelength than the signal and for a big wavelength difference between pump and signal. Also, another known noise process, the spontaneous parametric down-conversion of pump photons, is not relevant when

the pump has a higher wavelength than the signal. Both is the case for our method, the pump having a 800 nm higher wavelength than the signal for the conversion of 900-nm light and a 550-nm higher wavelength for the conversion of 1145-nm light described in the next section.

Regarding the sensitivity, our streak camera has a quantum efficiency of 0.72% at 900 nm and 8.16% at 590 nm, corresponding to a cathode radiant sensitivity of 5.22 mA/W and 38.84 mA/W, respectively. Multiplied by the 5% internal efficiency for 70-mW pump power, this gives 0.4% effective quantum efficiency for the converted light or 2.9 mA/W effective radiant sensitivity, without additional losses and coupling loss. (Note that for calculating the effective radiant sensitivity for the converted light, it is necessary to take the wavelength into account since the radiant sensitivity relates to the power instead of

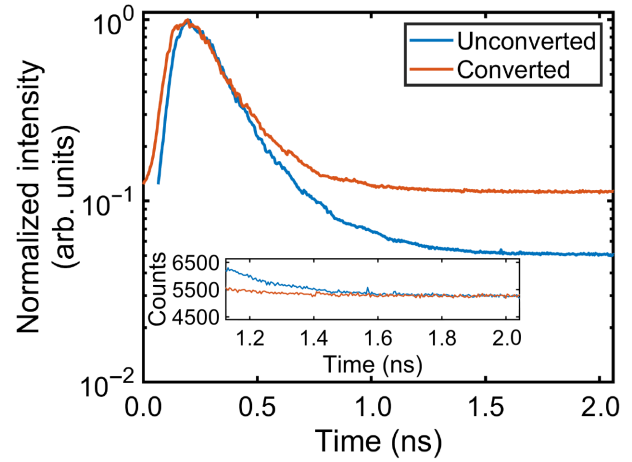


FIG. 6. The main plot depicts a cut through the streak-camera image along the spatial position of maximum intensity without background subtraction at 6-mW excitation power for the unconverted (blue) and the converted (red) signal in order to compare the dynamic range. The intensity is normalized. The inset shows both pulses for long times without intensity normalization in order to compare the background.

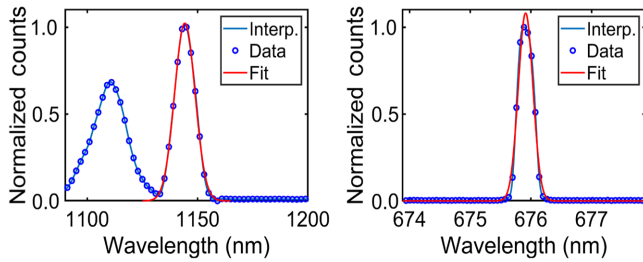


FIG. 7. Original (left) and converted (right) spectra of the 1145-nm laser light. Blue dots, data; red line, Gaussian fit; blue line, interpolant as guide for the eye. The intensities are normalized. They are not directly comparable due to different spectrometers and losses in the setup.

the photon number: effective radiant sensitivity = radiant sensitivity @ 590 nm  $\times$  internal conversion efficiency  $\times$  900 nm/590 nm.) When multiplying with the maximum observed internal efficiency of 14%, this gives 1.14% effective quantum efficiency for the converted light or 8.3 mA/W effective radiant sensitivity. This is not a major improvement; however, the conversion of 900-nm light is shown primarily to prove that the temporal shape is preserved.

#### IV. CONVERSION OF 1145-NM LIGHT

While the previous results validate the capability of our up-conversion process by converting wavelengths where streak cameras still possess small, but nonzero efficiency, the final goal is to convert wavelengths that are almost invisible for streak cameras. To achieve this, we design an optimized type-II SFG process with a poling period of 7  $\mu$ m, which combines light at 1150 nm with a pump at around 1700 nm to generate converted light at around 686 nm. To prove the applicability of this process, we convert test light from a continuous-wave diode laser (Toptica TA Pro) at 1145 nm, having a linewidth below 1 MHz. The setup is similar to the one shown in Fig. 2, but the pump is now set to 1649.2 nm to fulfil the phase-matching condition. The resulting spectra are shown in Fig. 7.

The unconverted signal consists of a broad emission around 1110 nm, produced by the ASE of the diode laser, and a peak of coherent emission at 1145 nm. Its broad FWHM of 11 nm is determined by the resolution of 5 nm of the EPP2000-NIR-InGaAs spectrometer, whereas the original laser linewidth lies below 1 MHz and cannot be resolved. The converted signal has a peak at 675.9 nm with a FWHM of 0.3 nm. It should, in fact, have the same width as the input laser since we are using a cw pump; however, this cannot be resolved by the spectrometer. We observe again that the central peak is converted to the desired output wavelength. Furthermore, as before, side peaks are suppressed, demonstrating the selective nature of the conversion.

Let us briefly discuss the effect of conversion at this wavelength for streak cameras. At the converted wavelength 676 nm, a S-25 photocathode has ca. 30 mA/W radiant sensitivity [27], corresponding to a quantum efficiency of 5.5%. In contrast to that, at 1145 nm, S1 photocathodes, which are better for the infrared, have a radiant sensitivity of ca. 0.1 mA/W [27], corresponding to a quantum efficiency of 0.011%, while InP/(In, Ga)As photocathodes have a radiant sensitivity of ca 1 mA/W at 1145 nm [28] or a quantum efficiency of 0.11%. Thus, when comparing a measurement of the converted signal with a S-25 to a measurement of the original signal with a S-1 photocathode, we gain a factor of ca. 550 regarding the quantum efficiency; when comparing to an InP/(In, Ga)As photocathode, the factor is still 55. Assuming an internal conversion efficiency of 14% as demonstrated in the proof-of-concept experiment, the effective radiant sensitivity for the converted light is  $30 \text{ mA/W} \times 14\% \times 1145 \text{ nm}/676 \text{ nm} = 7.1 \text{ mA/W}$  and the effective quantum efficiency is 0.77%. The system can accept up to 97% additional loss in the case of a S-1 photocathode and up to 74% additional loss in the case of an InP/(In, Ga)As photocathode to still outperform direct streak-camera detection twofold at this wavelength. We note that this big loss resilience emphasizes the strength of combining SFG with streak-camera detection for near- to midinfrared wavelengths: even for nonoptimized systems, as would be the case in real-world applications, one finds a significant performance enhancement while retaining all the upsides of streak-camera detection for temporal signal analysis.

#### V. CONCLUSION

We demonstrate that careful design of frequency-conversion processes can enhance quantum dot technologies. In particular, we design and experimentally confirm two SFG processes that preserve the temporal properties of quantum dot emission while converting it to the visible range, where streak cameras can be used at higher efficiencies. Overall, we demonstrate our system to achieve up to a twofold increase in the detection efficiency of quantum dots at 900 nm and a big enhancement for emission at 1150 nm while maintaining spectral properties. The system is resilient to losses and already outperforms S-1 and InP/(In, Ga)As photocathodes for telecom signal detection. Furthermore, the SFG process acts as a spectral and polarization filter for the quantum dot emission, thanks to the spatial single-mode propagation of the waveguides, the type-II conversion process between orthogonal polarizations and the transfer function. Finally, we would like to emphasize the major strength of our SFG technique, that is directly reproducing the sought-after pulse shape without any need to deconvolute the signal or scan a delay line, combined with the high time resolution of ca. 2 ps of the streak camera.

To sum up, alternative techniques for time-resolved measurements of weak signals in the infrared often rely on time-correlated single-photon counting, where detectors have time resolutions around 100 ps [15,36] and mostly lose efficiency in the infrared. Most promising are superconducting nanowire detectors, which usually have time resolutions around 20 ps or more [15,30] but are not always available because they require cryogenic cooling. On the other hand, up-conversion combined with SPADs or similar detectors has been demonstrated, e.g., in Ref. [34] but is still limited by the time resolution of those detectors. Up-conversion with a pulsed pump can have a better time resolution given by the pump-pulse duration but requires scanning a delay line and high acquisition times. Compared to these alternatives, our technique of up-conversion plus streak camera delivers a fast acquisition time, no scanning of a delay line, and a high time resolution of 2 ps. Furthermore, the acceptance bandwidth of the up-conversion process can, in principle, be designed to be as big as several 100 nms. In that case, the streak camera can provide a simultaneous measurement of temporal and spectral waveforms, which is a sought-after characterization tool in materials science for optics in the telecommunication range. Thus, our technique provides a complement to other methods when a streak camera is available as it is in many labs and high time resolution is required, presenting a starting point for further applications in the spectroscopy of infrared lightsources.

## ACKNOWLEDGMENTS

The authors would like to thank Christian Schneider and Sven Höfling for providing the microlaser sample. We gratefully acknowledge funding through the Deutsche Forschungsgemeinschaft (DFG, German Research Foundation) via the transregional collaborative research center TRR 142 (Project C01, Grant No. 231447078).

- [1] N. Somaschi, V. Giesz, L. De Santis, J. C. Loredo, M. P. Almeida, G. Hornecker, S. L. Portalupi, T. Grange, C. Antón, and J. Demory, *et al.*, Near-optimal single-photon sources in the solid state, *Nat. Photon.* **10**, 340 (2016).
- [2] C. Lüders, M. Pukrop, E. Rozas, C. Schneider, S. Höfling, J. Sperling, S. Schumacher, and M. Aßmann, Quantifying Quantum Coherence in Polariton Condensates, *PRX Quantum* **2**, 030320 (2021).
- [3] A. Othonos, Probing ultrafast carrier and phonon dynamics in semiconductors, *J. Appl. Phys.* **83**, 1789 (1998).
- [4] K. Zhang, D. Zhao, J. Wang, L. Zhang, M. Zou, Y. Guo, S. Wang, and B. Zou, Bosonic Lasing of Collective Exciton Magnetic Polarons in CuCl<sub>2</sub>-Doped CdS Nanoribbons: Implications for Quantum Light Sources, *ACS Appl. Nano Mater.* **3**, 5019 (2020).
- [5] F. Jahnke, C. Gies, M. Aßmann, M. Bayer, H. A. M. Leymann, A. Foerster, J. Wiersig, C. Schneider, M.

Kamp, and S. Höfling, Giant photon bunching, superradiant pulse emission and excitation trapping in quantum-dot nanolasers, *Nat. Commun.* **7**, 11540 (2016).

- [6] M. Nasu, K. Kawamura, T. Yoshida, J. Ishihara, and K. Miyajima, Influences of quantum fluctuation on superfluorescent spectra observed by single-shot measurement for semiconductor quantum dots, *Appl. Phys. Express* **13**, 062005 (2020).
- [7] J. A. Armstrong, Measurement of picosecond laser pulse widths, *Appl. Phys. Lett.* **10**, 16 (1967).
- [8] M. E. Anderson, A. Monmayrant, S.-P. Gorza, P. Wasylczyk, and I. A. Walmsley, SPIDER: A decade of measuring ultrashort pulses, *Laser Phys. Lett.* **5**, 259 (2008).
- [9] D. J. Kane and R. Trebino, Characterization of arbitrary femtosecond pulses using frequency-resolved optical gating, *IEEE J. Quantum Electron.* **29**, 571 (1993).
- [10] R. Hanbury Brown and R. Q. Twiss, Correlation between photons in two coherent beams of light, *Nature* **177**, 27 (1956).
- [11] E. Gilabert, A. Declémé, and C. Rullière, Picosecond fluorimeter using the optical Kerr effect for the direct and automatic recording of a whole time-resolved emission spectrum, *Rev. Sci. Instrum.* **58**, 2049 (1987).
- [12] H. Mahr and M. D. Hirsch, An optical up-conversion light gate with picosecond resolution, *Opt. Commun.* **13**, 96 (1975).
- [13] A. O. C. Davis, V. Thiel, M. Karpiński, and B. J. Smith, Measuring the Single-Photon Temporal-Spectral Wave Function, *Phys. Rev. Lett.* **121**, 083602 (2018).
- [14] A. Campillo and S. Shapiro, Picosecond streak camera fluorometry - A review, *IEEE J. Quantum Electron.* **19**, 585 (1983).
- [15] R. H. Hadfield, Single-photon detectors for optical quantum information applications, *Nat. Photon.* **3**, 696 (2009).
- [16] M. Aßmann, F. Veit, M. Bayer, M. van der Poel, and J. M. Hvam, Higher-order photon bunching in a semiconductor microcavity, *Science* **325**, 297 (2009).
- [17] J. Wiersig, C. Gies, F. Jahnke, M. Aßmann, T. Berstermann, M. Bayer, C. Kistner, S. Reitzenstein, C. Schneider, S. Höfling, A. Forchel, C. Kruse, J. Kalden, and D. Hommel, Direct observation of correlations between individual photon emission events of a microcavity laser, *Nature* **460**, 245 (2009).
- [18] L. Gao, J. Liang, C. Li, and L. V. Wang, Single-shot compressed ultrafast photography at one hundred billion frames per second, *Nature* **516**, 74 (2014).
- [19] N. Takemura, J. Omachi, and M. Kuwata-Gonokami, Fast periodic modulations in the photon correlation of single-mode vertical-cavity surface-emitting lasers, *Phys. Rev. A* **85**, 053811 (2012).
- [20] J. Schmutzler, T. Kazimierczuk, Ö. Bayraktar, M. Aßmann, M. Bayer, S. Brodbeck, M. Kamp, C. Schneider, and S. Höfling, Influence of interactions with noncondensed particles on the coherence of a one-dimensional polariton condensate, *Phys. Rev. B* **89**, 115119 (2014).
- [21] A. F. Adiyatullin, M. D. Anderson, P. V. Busi, H. Abbaspour, R. André, M. T. Portella-Oberli, and B. Deveaud, Temporally resolved second-order photon correlations of exciton-polariton Bose-Einstein condensate formation, *Appl. Phys. Lett.* **107**, 221107 (2015).

- [22] A. F. Adiyatullin, M. D. Anderson, H. Flayac, M. T. Portella-Oberli, F. Jabeen, C. Ouellet-Plamondon, G. C. Sallen, and B. Deveaud, Periodic squeezing in a polariton Josephson junction, *Nat. Commun.* **8**, 1329 (2017).
- [23] T. Kazimierczuk, J. Schmutzler, M. Aßmann, C. Schneider, M. Kamp, S. Höfling, and M. Bayer, Photon-Statistics Excitation Spectroscopy of a Quantum-Dot Micropillar Laser, *Phys. Rev. Lett.* **115**, 027401 (2015).
- [24] B. Schmidt, S. Laimgruber, W. Zinth, and P. Gilch, A broadband Kerr shutter for femtosecond fluorescence spectroscopy, *Appl. Phys. B* **76**, 809 (2003).
- [25] K. Appavoo and M. Y. Sfeira, Enhanced broadband ultrafast detection of ultraviolet emission using optical Kerr gating, *Rev. Sci. Instrum.* **85**, 055114 (2014).
- [26] M. Allgaier, V. Ansari, C. Eigner, V. Quiring, R. Ricken, J. M. Donohue, T. Czeriuik, M. Aßmann, M. Bayer, B. Brecht, and C. Silberhorn, Streak camera imaging of single photons at telecom wavelength, *Appl. Phys. Lett.* **112**, 031110 (2018).
- [27] HAMAMATSU PHOTONICS K.K., Systems Division, Universal Streak Camera C10910 series, (2018).
- [28] HAMAMATSU PHOTONICS K.K., Systems Division, NIR Streak Camera C11293-02, (2015).
- [29] B. Korzh, *et al.*, Demonstration of sub-3 ps temporal resolution with a superconducting nanowire single-photon detector, *Nat. Photon.* **14**, 250- (2020).
- [30] I. E. Zadeh, J. Chang, J. W. N. Los, S. Gyger, A. W. Elshaari, S. Steinhauer, S. N. Dorenbos, and V. Zwiller, Superconducting nanowire single-photon detectors: A perspective on evolution, state-of-the-art, future developments, and applications, *Appl. Phys. Lett.* **118**, 190502 (2021).
- [31] Y.-Z. Ma, J. Stenger, and J. Zimmermann, Ultrafast carrier dynamics in single-walled carbon nanotubes probed by femtosecond spectroscopy, *J. Chem. Phys.* **120**, 3368 (2004).
- [32] D. C. Dai and A. P. Monkman, Observation of superfluorescence from a quantum ensemble of coherent excitons in a ZnTe crystal: Evidence for spontaneous Bose-Einstein condensation of excitons, *Phys. Rev. B* **84**, 115206 (2011).
- [33] A. Delteil, C. T. Ngai, T. Fink, and A. İmamoğlu, Second-order photon correlation measurement with picosecond resolution using frequency upconversion, *Opt. Lett.* **44**, 3877 (2019).
- [34] M. T. Rakher, L. Ma, O. Slattery, X. Tang, and K. Srinivasan, Quantum transduction of telecommunications-band single photons from a quantum dot by frequency upconversion, *Nat. Photon.* **4**, 786- (2010).
- [35] M. T. Rakher, L. Ma, M. Davanço, O. Slattery, X. Tang, and K. Srinivasan, Simultaneous Wavelength Translation and Amplitude Modulation of Single Photons from a Quantum Dot, *Phys. Rev. Lett.* **107**, 083602 (2011).
- [36] D. Bronzi, F. Villa, S. Tisa, A. Tosi, and F. Zappa, SPAD figures of merit for photon-counting, photon-timing, and imaging applications: A review, *IEEE Sens. J.* **16**, 3 (2016).
- [37] A. Eckstein, B. Brecht, and C. Silberhorn, A quantum pulse gate based on spectrally engineered sum frequency generation, *Opt. Express* **19**, 13770 (2011).
- [38] P. A. Augstov and K. K. Shvarts, The temperature and light intensity dependence of photorefraction in LiNbO<sub>3</sub>, *Appl. Phys.* **21**, 191- (1980).
- [39] K. Lüdge, M. J. P. Bormann, E. Malié, P. Hövel, M. Kuntz, D. Bimberg, A. Knorr, and E. Schöll, Turn-on dynamics and modulation response in semiconductor quantum dot lasers, *Phys. Rev. B* **78**, 035316 (2008).
- [40] J. S. Pelc, L. Ma, C. R. Phillips, Q. Zhang, C. Langrock, O. Slattery, X. Tang, and M. M. Fejer, Long-wavelength-pumped upconversion single-photon detector at 1550 nm: performance and noise analysis, *Opt. Express* **19**, 21445 (2011).